



Obrabotka metallov - Metal Working and Material Science

Journal homepage: http://journals.nstu.ru/obrabotka_metallov



Formation and investigation of the properties of FeWCrMoBC metallic glass coatings on carbon steel

Alexander Burkov^a, Leonid Konevtsov^{b,*}, Maxim Dvornik^c, Sergey Nikolenko^d, Maria Kulik^e

Federal State Budgetary Institution of Science Institute of Materials Science of the Khabarovsk Scientific Center of the Far Eastern Branch of the Russian Academy of Sciences, 153 Tihookeanskaya st., Khabarovsk, 680042, Russian Federation

^a  <https://orcid.org/0000-0002-5636-4669>,  burkovalex@mail.ru; ^b  <https://orcid.org/0000-0002-8820-6358>,  konevts@narod.ru;
^c  <https://orcid.org/0000-0002-1216-4438>,  maxxxx80@mail.ru; ^d  <https://orcid.org/0000-0003-4474-5795>,  nikola1960@mail.ru;
^e  <https://orcid.org/0000-0002-4857-1887>,  marijka80@mail.ru

ARTICLE INFO

Article history:

Received: 01 September 2023
 Revised: 19 September 2023
 Accepted: 19 October 2023
 Available online: 15 December 2023

Keywords:

Metallic glass
 Coating
 Electric discharge alloying
 High-temperature resistance
 Wettability
 Coefficient of friction
 Wear resistance

Funding

The work was carried out within the framework of the state task of the Ministry of Science and Higher Education of the Russian Federation No. 075-01108-23-01 (topic No. 123020700174-7).

Acknowledgements

Research were partially conducted at core facility “Structure, mechanical and physical properties of materials”.

ABSTRACT

Introduction. To obtain metallic glass coatings it is necessary to achieve high cooling rates of melt. *FeWCrMoBC* composition has high melt viscosity and sufficient glass-forming ability to fix of the amorphous state at cooling rates implemented by electric discharge alloying with the use of a crystalline electrode. **The purpose of the work** is one-stage deposition of amorphous coating by electric discharge alloying, using crystalline anode *FeWCrMoBC*, prepared by casting and studying the properties of modified surface of carbon steel: wettability, high-temperature resistance, tribological properties. **Methods and Results.** The structure of anode and coatings was investigated by X-ray diffraction analysis in CuK_{α} radiation on a *DRON-7* diffractometer. In contrast to the X-ray patterns of the anode material, sharp *Bragg* reflexes were not observed on the X-ray patterns of the coatings, but a wide halo was present in the range of angles $2\theta = 40\text{--}50^\circ$, which indicates its amorphous structure. The cyclic high-temperature resistance test was carried out at 700°C for 100 hours. The wear rate and coefficient of friction of the specimens were studied under dry sliding friction at a speed of 0.47 m/s at a load of 25 N with the use of a counterbody made of high-speed steel *M45*. The influence of the discharge pulse duty cycle on the character of mass transfer (anode erosion, cathode weight gain, mass transfer coefficient) during coating formation was investigated. With a decrease in the duty cycle of the discharge pulses up to 9 times, the erosion of the anode increased up to 5 times, and the cathode mass gain increased up to 2.2 times. The maximum mass-transfer coefficient was achieved at the highest duty cycle. An increase in a number of surface properties of carbon steel after coating was observed: the hardness of the surface of the specimens increased by 2.3–2.6 times; the average thickness of the coatings was in the range of 56–80.6 μm ; the wetting angle was in the range of $108.4\text{--}121.3^\circ$; the coefficient of friction decreased by 1.2–1.4 times; the wear resistance increased by 2–3.3 times; oxidizability in air decreased by 14–18 times. **Scope and Conclusions.** The achieved higher properties (hardness, wear resistance, high-temperature resistance, and hydrophobicity) of the executive surfaces of parts made of carbon steel after deposition of the proposed coatings can be used in various branches of engineering production. The results of the work confirmed the possibility of deposition of metallic glass coatings by electric discharge alloying with the use of cast anode material *FeWCrMoBC* on carbon steel.

For citation: Burkov A.A., Konevtsov L.A., Dvornik M.I., Nikolenko S.V., Kulik M.A. Formation and investigation of the properties of FeWCrMoBC metallic glass coatings on carbon steel. *Obrabotka metallov (tehnologiya, oborudovanie, instrumenty) = Metal Working and Material Science*, 2023, vol. 25, no. 4, pp. 244–254. DOI: 10.17212/1994-6309-2023-25.4-244-254. (In Russian).

* Corresponding author

Konevtsov Leonid A., Ph.D. (Engineering), Senior researcher
 Federal State Budgetary Institution of Science
 Institute of Materials Science of the Khabarovsk Scientific Center
 of the Far Eastern Branch of the Russian Academy of Sciences,
 153 Tihookeanskaya st.,
 680042, Khabarovsk, Russian Federation
 Tel.: +7 (924) 105-97-46, E-mail: konevts@narod.ru

Introduction

The structure of metallic glasses (*MG*), by contrast with metals, is amorphous, characterized by the presence of short-distance order and the absence of long-distance order in the arrangement of atoms, which is characteristic of the atomic structure of supercooled melts. Due to this, bulk *MGs* have high elasticity comparable to polymers, increased *Young's* modulus [1–3]; magnetic properties [4], catalytic activity [5–7]; resistance to radiation and others. The production of bulk *MGs* with a thickness of more than 10 mm is currently difficult due to the requirement of high cooling rate of the material. Therefore, it is promising to apply *MG* coatings to impart properties to the executive surfaces of massive parts.

MGs and hardening coatings formed from iron-based *MG* have increased hardness [8], increased wear resistance [1, 9, 10], lower friction coefficients [11], high-temperature resistance [12, 13] corrosion resistance [2, 14–16] and other properties [17, 18] compared with the substrate material.

To obtain *MG* coatings, it is necessary to achieve high melt cooling rates. *FeWCrMoBC* composition contains elements with significantly different atomic radii, due to this melt has high viscosity, which makes it difficult to move atoms to build the crystal structure, and therefore does not require extremely high cooling rates for the formation of *MG* by contrast with pure metals. Electric discharge alloying (*EDA*) provides sufficiently high cooling rates (10^5 – 10^7 K/s) [19, 20] of such materials in the melt micro-bath to fix the amorphous state. *EDA* is based on the phenomenon of polar transfer of material from anode to cathode during the flow of microsecond low-voltage electrical discharges [21]. As a consequence, *EDA* can utilize a crystalline electrode-anode for one-step deposition of an amorphous coating [22]. Previously, we obtained similar coatings using electrodes (anodes) prepared by powder metallurgy. The purpose of this work is a one-stage deposition of an amorphous coating by *EDA* using crystalline anode material *FeWCrMoBC* prepared by casting with a higher iron concentration and the investigation of wettability, high-temperature resistance and tribological properties of coatings.

Research methods

In laboratory conditions of *KHFIC IM FEB RAS* the electrode material of $Fe_{31}W_{10}Cr_{22}Mo_7B_{12}C_{18}$ composition from a mixture of powders was created by casting method (table 1). The powders were mixed and poured into a corundum crucible, which was placed in a muffle furnace and heated up 1,200 °C. After soaking for 15 minutes, the crucible was removed from the furnace and the melt was poured onto a steel plate at room temperature. The obtained material was cut into $4 \times 4 \times 30$ mm³ rectangles, which served as electrodes.

Table 1

Composition of the powder mixture for the anode preparation

Concentration, wt.%	B_4C	<i>W</i>	<i>Mo</i>	<i>Fe</i>	<i>Cr</i>	<i>C</i>
	2.97	32.82	11.4	29.8	19.95	3.06

The power pulse generator was used during *EDA* with discharge current 195 ± 10 A; voltage 40 ± 5 V and the following processing modes (table 2), where: $D = 1/S$ is a duty cycle; $S = T/\tau$ is a pulse on-off time; T is a pulse period; τ is a pulse duration.

The coatings were deposited on the surface of the cathode specimens made of *Steel 35* in the form of a cylinder with a height of 5 mm and a diameter of 12 mm during 6 min/cm² in air. The values of anode erosion and cathode weight gain were determined with using electronic scales *BSM-120* with an accuracy of 0.1 mg.

An X-ray diffractometer “*DRON-7*” in $Cu-K_\alpha$ radiation was used to study the structure of the specimens. The hardness of the coatings was measured on a *PMT-3M* microhardness tester at a load of 0.5 N using the *Vickers* method. Wear resistance and coefficient of friction of coatings were investigated according to

Modes of electric discharge alloying

Specimen designation	MC50	MC150	MC450
S	50	150	450
T , ms	2.5	7.5	22.5
τ , μ s	50	50	50
Number of pulses	144,000	48,000	16,000

ASTM G99-17 standard under dry sliding friction with the use of a disk counterbody made of *M45* high-speed steel (65 HRC) at a speed of 0.47 m/s at a load of 25 N. Cyclic high-temperature resistance tests were carried out in a muffle furnace at 700 °C in air. The specimens in the form of a cube with an edge of 6 mm, with a coating on each face, were held at a given temperature for ~6 h, then cooled in an desiccator to room temperature. The total testing time was 100 h. During the oxidation resistance test, the specimens were placed in ceramic crucibles to account in the mass of formed oxides.

The wetting edge angle was determined by the “*sessile drop*” method [23]. Free surface energy was determined by wetting with distilled water, ethanol (C_2H_5OH), sodium chloride solution (6M *NaCl*), formic acid (CH_2O_2). The free surface energy was calculated using the theoretical model [24]:

$$Y_{SL} = Y_S + Y_L - 2\sqrt{Y_S Y_L} [1 - \beta_1(Y_L - Y_S)^2] \quad (1)$$

which in combination with *Young's* equation gives:

$$Y_L(1 + \cos \Theta) = 2\sqrt{Y_S Y_L} [1 - \beta_1(Y_L - Y_S)^2], \quad (2)$$

where β_1 is equal to 0.0001057 (m/mN)².

Then equation (2) allows, with some assumption, to estimate the free surface energy (Y_s) from the measurement of the contact angle of a liquid with known surface tension Y_L .

Results and its discussion

The study of mass transfer in the *EDA* process is important for establishing the fact of cathode weight increase and the value of specific cathode weight gain, especially when using new anode-cathode electrode pairs, since the coating thickness can be considered as a function of cathode weight gain over time [25]. Fig. 1 shows the dependences of anode erosion, the value of specific cathode weight gain and total mass-transfer coefficient on the *EDA* time.

The anode electrical erosion curves increased linearly over the *EDA* time (fig. 1, *a*), the greatest anode erosion was observed at the highest duty cycle. With increasing the duty cycle by 3 and 9 times, the erosion values decreased in 1.2 and 5 times, respectively. Thus, the anode erosion depends nonlinearly on the number of pulses sent by the generator. With an increase in the duty cycle due to a reduction in the number of discharge pulses, the values of summarized cathode weight gain decreased by 1.5 and 2.2 times, respectively (fig. 1, *b*). The cathode weight gain monotonically increased during the first 4 minutes of *EDA*, and in the following 5–6 minutes a slowdown in the weight gain was observed due to the approaching the brittle fracture threshold [21]. In accordance with this, the mass-transfer coefficient ($C_{t,c}$) gradually decreased with increasing *EDA* time for all modes. At minimum duty cycle, $C_{t,c}$ was twice as large compared to the other modes (fig. 1, *c*). This is explained by the decrease in the number of discharges per unit of the surface being treated per unit of time, at which the electrodes cool down to lowest temperatures. When the initial temperature of the anode decreases, the volume of melt microbath decreases and, accordingly, erosion at a single discharge decreases.

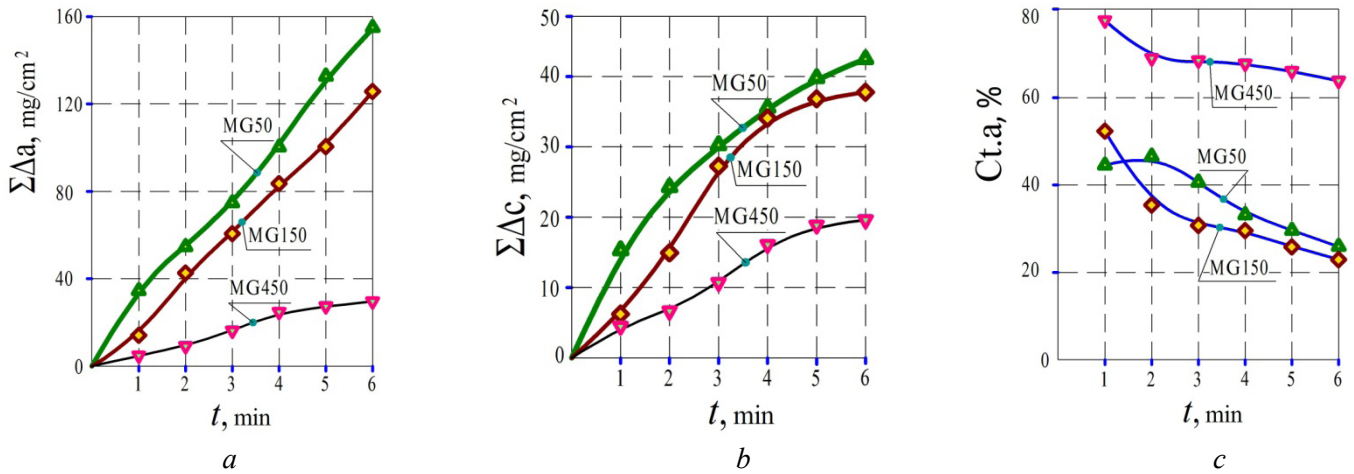


Fig. 1. Kinetics of mass transfer during EDA with different pulse intensity:

erosion of the anode $\Sigma\Delta a$, mg/cm^2 (a); cathode weight gain $\Sigma\Delta c$, mg/cm^2 (b); average mass-transfer coefficient $\Sigma C_{t,a}$ of specimens MS50, MS150, MS450 (c)

X-ray diffraction analysis showed that in the anode composition of $Fe_{31}W_{10}Cr_{22}Mo_7B_{12}C_{18}$ contains phases of ferrochrome ($Fe-Cr$), borides and carbides: $Fe_{23}B_4$, $MoFeB_2$, $\alpha-WC$, Mo_2C (fig. 2, a), which were not present in the composition of the powder mixture before melting. This indicates the intensive chemical reactions during the holding process of the composition presented in table 1 at 1,200 °C. Whereas on the X-ray spectra of coatings obtained with its use, no sharp Bragg reflexes are observed, and there is a wide halo in the range of angles $2\Theta = 40-50^\circ$, indicating the amorphous structure of the deposited layers.

The main characteristics of EDA coatings on Steel 35 using $Fe_{31}W_{10}Cr_{22}Mo_7B_{12}C_{18}$ anode are summarized in table 3. The average thickness of the coatings was in the range of 56–80 μm , with a maximum at specimen MG50. The surface roughness of the coatings in terms of R_a parameter was in range of 6.79–5.46 μm with the increase in the duty ratio. The water contact angle ranged from 108.4° to 121.3° (fig. 2, b), which is higher compared to Steel 35 (57.5°). The free surface energy of the coatings was calculated and it was in the range of 29.9–32.3 mJ/m^2 , which is lower compared to the original base material (39.97 mJ/m^2). This suggests that the application of $Fe_{31}W_{10}Cr_{22}Mo_7B_{12}C_{18}$ coatings can reduce the surface activity of Steel 35 to contaminants and corrosion [26].

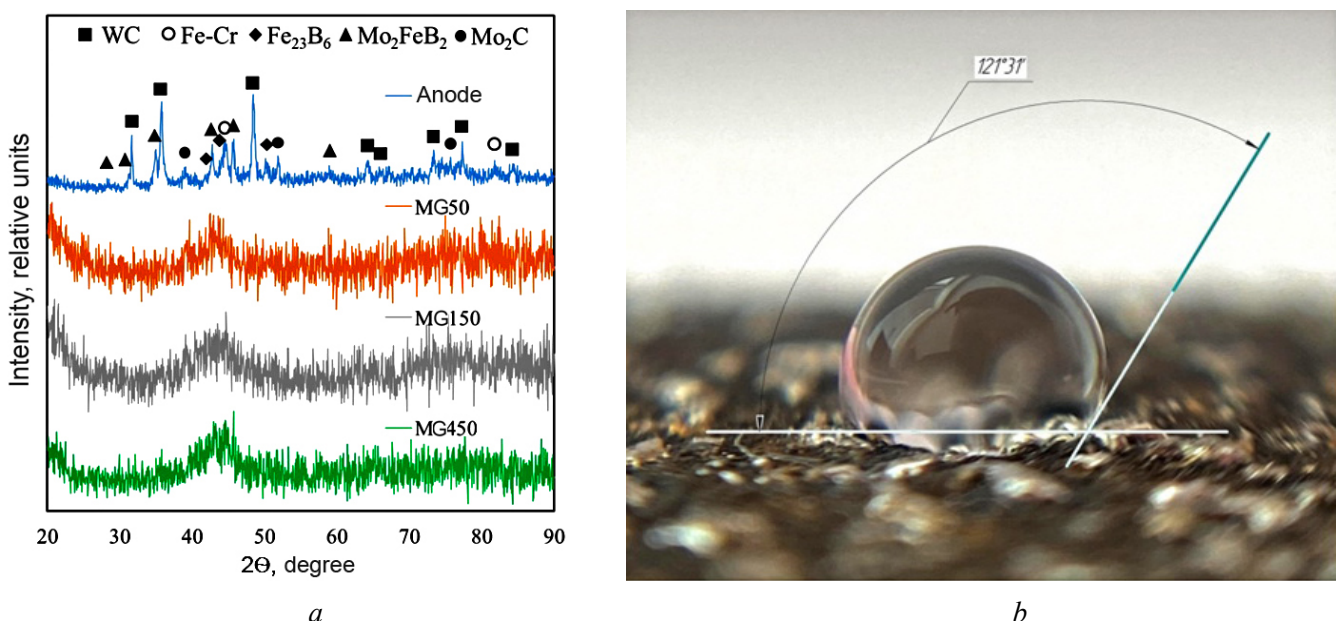


Fig. 2. X-ray diffraction patterns of the anode of the $Fe_{31}W_{10}Cr_{22}Mo_7B_{12}C_{18}$ composition (a); wettability of the coating surface of the MG450 specimen (b)

Characteristics of the deposited coatings

Parameter	Steel 35	MC50	MC150	MC450
Coating thickness $h_{a.th}$, μm		80.6	77.1	56.1
Roughness Ra , μm	3.2 ± 1.5	6.79 ± 1.54	7.34 ± 1.74	5.46 ± 0.92
Wetting angle, $^\circ$ (degree)	57.5 ± 3.8	111.9 ± 6.1	108.4 ± 7.3	121.3 ± 4.9
Surface energy	39.97 ± 17.6	32.3 ± 18.7	33.1 ± 17	29.9 ± 15.5

The microhardness of $Fe_{31}W_{10}Cr_{22}Mo_7B_{12}C_{18}$ coatings was in the range of 6.65–7.56 GPa (fig. 3), which is 2.3–2.6 times higher than that of uncoated Steel 35, and also exceeds the values obtained by other researchers for $MG Fe_{47}Cr_{20}Mo_{10}W_6C_{15}B_6Y_2$ (1.28 GPa) [27], is commensurate with the values for $MG Zr_{50}Cu_{28}Al_{14}Ni_8$ (7.2 GPa); $Cu_{48}Zr_{42}Al_6Ti_4$ (4.0 GPa); $Hf_{46}Cu_{45}Al6Ti_3$ (7.7 GPa) [28], inferior to the data obtained for $MG Fe_{65}Ti_{13}Co_8Ni_7B_6Nb_1$ (11.6 GPa) [27] and $MG Fe_{41}Cr_8Ni_8Mo_8Co_8C_{16}B_{11}$ (10–15 GPa) [29].

The friction coefficient values of the studied coated specimens monotonically decreased from 0.49 to 0.44 with increasing pulse on-off time from 50 to 450 (fig. 4, a). The friction coefficient of the coated specimens was smaller than that of uncoated Steel 35 (0.6) and was commensurate with the previously obtained data for $Zr_{35}Ti_{30}Cu_{8.25}Be_{26.75}$ (0.43–0.6) [11], slightly inferior to the data obtained for $Zr_{56.2}Ti_{3.8}Nb_{5.0}Cu_{6.9}Ni_{5.6}Be_{12.5}$ (0.27–0.35) [30]. However, the latter MGs contain beryllium, which is extremely toxic.

The present relative values of wear rate of specimens with coatings was in the range from 0.86×10^{-5} to $1.45 \times 10^{-5} \text{ mm}^3/(\text{Nm})$ (fig. 4, b). Thus, the use of $Fe_{31}W_{10}Cr_{22}Mo_7B_{12}C_{18}$ metallic glass coatings can increase the wear resistance of the surface of Steel 35 by 2.0–3.3 times. The lowest values of wear rate were shown by the coating obtained at the lowest pulse on-off time of 50.

The high-temperature resistance test of specimens characterizes not only the resistance of the coating material to oxidation, but also the continuity of the deposited layer. The mass change kinetics of specimens with $Fe_{31}W_{10}Cr_{22}Mo_7B_{12}C_{18}$ coatings (fig. 5, a, left scale) and uncoated Steel 35 (fig. 5, a; right scale) at temperature 700 °C is shown. The weight gain of the specimens is due to the fixation of oxygen on its

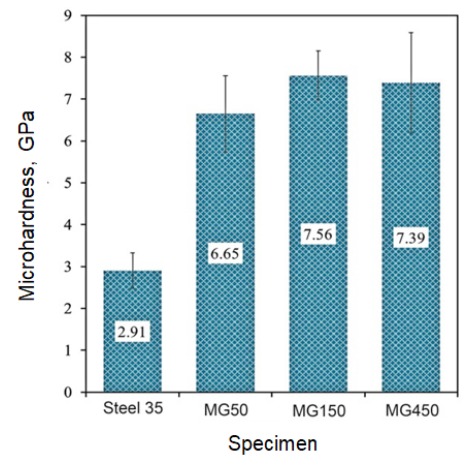


Fig. 3. Microhardness of coatings

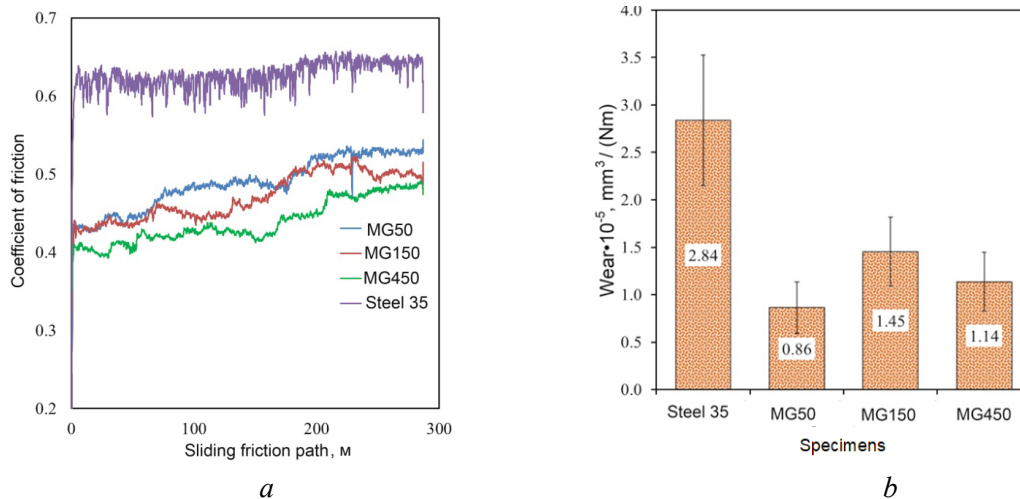


Fig. 4. Coefficient of friction (a) and wear (b) of coatings compared to Steel 35 at a load of 25 N

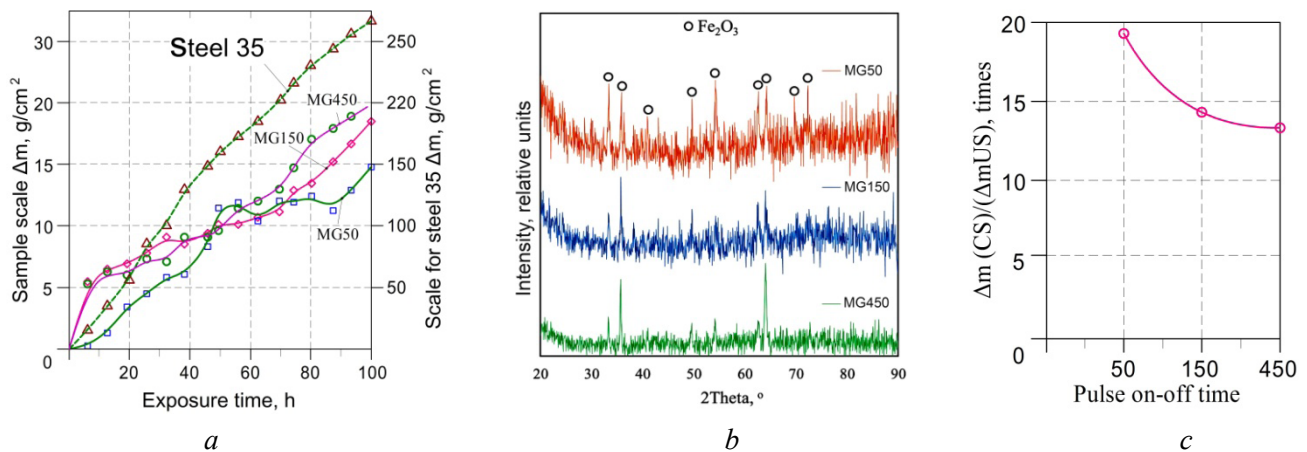


Fig. 5. High-temperature resistance of specimens at 700 °C as compared to uncoated *Steel 35*: kinetics of mass change Δm , g/cm^2 (a); X-ray diffraction analysis of the coating surface after high-temperature resistance tests (b); change in high-temperature resistance of coated specimen (CS) and uncoated specimen (US) from pulse on-off time (c)

surface in the form of hematite (fig. 5, b). During 100 hours of testing, the specimens with coatings from 13.5 to 18.8 times less subjected to oxidation than *Steel 35* due to limited oxygen contact with the steel substrate (fig. 5, c). The protective effect of the coatings increased with increasing the duty cycle, which is due to an increase in the specific number of discharges and, as a consequence, an increase in the thickness and continuity of the coatings.

Conclusions

1. The possibility of using the anode material of $\text{Fe}_{31}\text{W}_{10}\text{Cr}_{22}\text{Mo}_7\text{B}_{12}\text{C}_{18}$ composition prepared by casting method for obtaining EDA coating of MG on carbon steel is shown.
2. With increasing in the pulse duty cycle by 3 and 9 times, the values of erosion increased by 1.2 and 5 times; the cathode weight increased by 1.5 and 2.2 times, respectively. At the lowest EDA intensity, the mass-transfer coefficient of EDA was the greatest.
3. In the composition of the prepared electrode materials $\text{Fe}_{31}\text{W}_{10}\text{Cr}_{22}\text{Mo}_7\text{B}_{12}\text{C}_{18}$ composition the $\alpha\text{-WC}$, FeCr , Fe_{23}B_4 , Mo_2C , and MoFeB_2 phases were found, while no sharp Bragg reflections were observed in the XRD spectra of the coatings, and a broad halo was present in the range of angles $2\Theta = 40\text{--}50^\circ$, indicating the amorphous structure of metal glass.
4. The thickness of the coatings ranged from 56.1 to 80.6 μm , with roughness (R_a) from 5.46 to 7.34 μm . The coatings exhibited high water contact angle ranging from 108.4° to 121.3° , indicating high surface hydrophobicity of the developed coatings.
5. The friction coefficient of $\text{Fe}_{31}\text{W}_{10}\text{Cr}_{22}\text{Mo}_7\text{B}_{12}\text{C}_{18}$ metallic glass coatings was lower than that of carbon steel from 22 to 36 %. Its application allows to increase the wear resistance of carbon steel surface by 2.0–3.3 times. The highest values of wear resistance were shown by the coating obtained at highest duty cycle.
6. Application of $\text{Fe}_{31}\text{W}_{10}\text{Cr}_{22}\text{Mo}_7\text{B}_{12}\text{C}_{18}$ coatings allows to increase high-temperature resistance of carbon steel at temperature 700 °C by 13.5–18.8 times. The best high-temperature resistance was shown for coating obtained at lowest duty cycle of EDA.

References

1. Sivaraman R., Patra In., Zainab M.N., Hameed N.M., Alawsi T., Hashemi S. The effects of minor element addition on the structural heterogeneity and mechanical properties of ZrCuAl bulk metallic glasses. *Advances in Materials Science and Engineering*, 2022, vol. 2022, Art. 6528470. DOI: 10.1155/2022/6528470.
2. Chang J.C., Lee J.W., Lou B.S., Li C.L., Chu J.P. Effects of tungsten contents on the microstructure, mechanical and anticorrosion properties of Zr–W–Ti thin film metallic glasses. *Thin Solid Films*, 2015, vol. 584, pp. 253–256. DOI: 10.1016/j.tsf.2015.01.063.



3. Zhu K., Jiang W., Wu J., Zhang B. Effect of Mo on properties of the industrial Fe–B-alloy-derived Fe-based bulk metallic glasses. *International Journal of Minerals, Metallurgy and Materials*, 2017, vol. 24, pp. 926–930. DOI: 10.1007/s12613-017-1479-1.
4. Wang W.M., Zhang W.X., Gebert A., Mickel C., Schultz L. Microstructure and magnetic properties in Fe₆₁Co_{9-x}Zr₈Mo₅W_xB₁₇ (0 ≤ x ≤ 3) glasses and glass-matrix composites. *Metallurgical and Materials Transactions A*, 2009, vol. 40 (3), pp. 511–521. DOI: 10.1007/s11661-008-9706-z.
5. Wang J.Q., Liu Y.H., Chen M.W., Xie G.Q., Louzguine-Luzgin D.V., Inoue A., Perepezko J.H. Rapid degradation of azo dye by Fe-based metallic glass powder. *Advanced Functional Materials*, 2012, vol. 22 (12), pp. 2567–2570. DOI: 10.1002/adfm.201103015.
6. Wang X., Pan Y., Zhu Z., Wu J. Efficient degradation of rhodamine B using Fe-based metallic glass catalyst by Fenton-like process. *Chemosphere*, 2014, vol. 117, pp. 638–643. DOI: 10.1016/j.chemosphere.2014.09.055.
7. Zhang H., Hu Y., Hou G., An Y., Liu G. The effect of high-velocity oxy-fuel spraying parameters on microstructure, corrosion and wear resistance of Fe-based metallic glass coatings. *Journal of Non-Crystalline Solids*, 2014, vol. 406, pp. 37–44. DOI: 10.1016/j.jnoncrysol.2014.09.041.
8. Wang Y., Jiang S.L., Zheng Y.G., Ke W., Sun W.H., Wang J.Q. Effect of molybdenum, manganese and tungsten contents on the corrosion behavior and hardness of iron-based metallic glasses. *Materials and Corrosion*, 2014, vol. 65, pp. 733–741. DOI: 10.1002/maco.201206740.
9. Wu H., Lan X.-d., Liu Y., Li F., Zhang W.-d., Chen Z.-j., Zai X.-f., Zeng H. Fabrication, tribological and corrosion behaviors of detonation gun sprayed Fe-based metallic glass coating. *Transactions of Nonferrous Metals Society of China*, 2016, vol. 26 (6), pp. 1629–1637. DOI: 10.1016/S1003-6326(16)64271-1.
10. Wang Y., Ouyang G., Zhang L., Wu X., Zhang H., Wang S. Corrosion resistance of coating with Fe-based metallic glass powders fabricated by laser spraying. *Journal of Applied Sciences*, 2013, vol. 13 (9), pp. 1479–1483. DOI: 10.3923/jas.2013.1479.1483.
11. Li N., Xu E., Liu Z., Wang X., Liu L. Tuning apparent friction coefficient by controlled patterning bulk metallic glasses surfaces. *Scientific Reports*, 2016, vol. 6 (1), p. 39388. DOI: 10.1038/srep39388.
12. Hitit A., Şahin H. The effect of iron content on glass forming ability and thermal stability of Co–Fe–Ni–Ta–Nb–B–Si bulk metallic glass. *Metals*, 2017, vol. 7 (1), p. 7. DOI: 10.3390/met7010007.
13. Burkov A.A. Deposition of metallic glass coatings by electrospark processing in the medium of granules of Fe₃₉Ni₈Cr₇W₇Mo₇Co₂C₁₆B₁₄ composition. *Pis'ma o materialakh = Letters on materials*, 2017, vol. 7 (3), pp. 254–259. DOI: 10.22226/2410-3535-2017-3-254-259. (In Russian).
14. Zohdi H., Shahverdi H.R., Hadavi S.M. Effect of Nb addition on corrosion behavior of Fe-based metallic glasses in Ringer's solution for biomedical applications. *Electrochemistry Communications*, 2011, vol. 13 (8), pp. 840–843. DOI: 10.1016/j.elecom.2011.05.017.
15. Madinehei M., Brun P., Duarte M.J., Pined E., Klemm J., Renner F.U. Glass-formation and corrosion properties of Fe–Cr–Mo–C–B glassy ribbons with low Cr content. *Journal of Alloys and Compounds*, 2014, vol. 615, pp. S128–S131. DOI: 10.1016/j.jallcom.2013.12.245.
16. Sagasti A., Lopes A.C., Lasheras A., Palomares V., Carrizo J., Gutierrez J., Barandiaran J.M. Corrosion resistant metallic glasses for biosensing applications. *AIP Advances, Special Collection: 23rd Soft Magnetic Materials Conference*, 2018, vol. 8 (4), p. 047702. DOI: 10.1063/1.4994108.
17. Burkov A.A., Pyachin S.A., Ermakov M.A., Syuy A.V. In situ synthesis and characterization of Fe-based metallic glass coatings by electrospark deposition technique. *Journal of Materials Engineering and Performance*, 2017, vol. 26, pp. 901–908. DOI: 10.1007/s11665-016-2493-6.
18. Zhang C., Chu Z., Wei F., Qin W., Yang Y., Dong Y., Huang D., Wang L. Optimizing process and the properties of the sprayed Fe-based metallic glassy coating by plasma spraying. *Surface and Coatings Technology*, 2017, vol. 319, pp. 1–5. DOI: 10.1016/j.surfcoat.2017.03.063.
19. Liu L., Zhang C. Fe-based amorphous coatings: Structures and properties. *Thin Solid Films*, 2014, vol. 561, pp. 70–86. DOI: 10.1016/j.tsf.2013.08.029.
20. Li Q.H., Yue T.M., Guo Z.N., Lin X. Microstructure and corrosion properties of AlCoCrFeNi high entropy alloy coatings deposited on AISI 1045 steel by the electrospark process. *Metallurgical and Materials Transactions A*, 2013, vol. 44A, pp. 1767–1778. DOI: 10.1088/2051-672X/ab411b.
21. Lyashenko B.A., Podchernyaeva I.A., Konevtsov L.A., Kovalenko S.V., Kaminskii A.V. *Materialogiya pokrytii titanovykh splavov metodami fizikokhimii i elektroiskrovogo legirovaniya*. V 2 ch. Ch. 2. *EIL-pokrytiya* [Materialogy of coatings of titanium alloys by methods of physical chemistry and electrospark alloying. In 2 vol. Vol. 2. ESA coatings]. Khabarovsk, Pacific National University Publ., 2020. 347 p. ISBN 978-5-7389-3025-6.



22. Hasanabadi M.F., Ghaini F.M., Ebrahimnia M., Shahverdi H.R. Production of amorphous and nanocrystalline iron based coatings by electro-spark deposition process. *Surface and Coatings Technology*, 2015, vol. 270, pp. 95–101. DOI: 10.1016/j.surfcoat.2015.03.016.
23. Emelyanenko A.M., Boinovich L.B. Analysis of wetting as an efficient method for studying the characteristics of coatings and surfaces and the processes that occur on them: a review. *Inorganic Materials*, 2011, vol. 47 (15), pp. 1667–1675. DOI: 10.1134/S0020168511150064.
24. Schuster J.M., Schvezov C.E., Rosenberger M.R. Analysis of the results of surface free energy measurement of Ti_6Al_4V by different methods. *Procedia Materials Science*, 2015, vol. 8, pp. 732–741. DOI: 10.1016/j.mspro.2015.04.130.
25. Jamnapara N.I., Frangini S., Alphonsa J., Chauhan N.L., Mukherjee S. Comparative analysis of insulating properties of plasma and thermally grown alumina films on electrospark aluminide coated 9Cr steels. *Surface and Coatings Technology*, 2015, vol. 266, pp. 146–150. DOI: 10.1016/j.surfcoat.2015.02.028.
26. Li Y.C., Zhang W.W., Wang Y., Zhang X.Y., Sun L.L. Effect of spray powder particle size on the bionic hydrophobic structures and corrosion performance of Fe-based amorphous metallic coatings. *Surface and Coatings Technology*, 2022, vol. 437, p. 128377. DOI: 10.1016/j.surfcoat.2022.128377.
27. Liang D.D., Wei X.S., Chang C.T., Li J.W., Wang X.M., Shen J. Effect of W addition on the glass forming ability and mechanical properties of Fe-based metallic glass. *Journal of Alloys and Compounds*, 2018, vol. 731, pp. 1146–1150. DOI: 10.1016/j.jallcom.2017.10.104.
28. Negussie A.T., Chu J.P., Diyatmik W., Lee C.M., Yu C., Shen Y.L., Hsueh C.H. Annealing-induced indentation recovery in thin film metallic glasses: Effects of indenter tip geometry, film thickness and film composition. *Surface and Coatings Technology*, 2015, vol. 261, pp. 350–355. DOI: 10.1016/j.surfcoat.2014.10.068.
29. Burkov A.A., Krutikova V.O. Osazhdenie amorfnnykh uprochnyayushchikh pokrytii elektroiskrovoi obrabotkoi v smesi kristallicheskikh granul [Deposition of amorphous hardening coatings by electrospark treatment in a crystalline granule mixture]. *Izvestiya vuzov. Poroshkovaya metallurgiya i funktsional'nye pokrytiya = Powder Metallurgy and Functional Coatings*, 2019, no. 2, pp. 57–67. DOI: 10.17073/1997-308X-2019-2-57-67.
30. Ayyagari A., Hasannaemi V., Arora H., Mukherjee S. Electrochemical and friction characteristics of metallic glass composites at the microstructural length-scales. *Scientific Reports*, 2018, vol. 8 (1), pp. 906. DOI: 10.1038/s41598-018-19488-7.

Conflicts of Interest

The authors declare no conflict of interest.

© 2023 The Authors. Published by Novosibirsk State Technical University. This is an open access article under the CC BY license (<http://creativecommons.org/licenses/by/4.0>).